Garbanzo-Salas and Hocking
Earth, Planets and Space (2019) 71:6
https://doi.org/10.1186/s40623-019-0985-y

Earth, Planets and Space

FRONTIER LETTER

Characterization of atmospheric structures observed by a VHF MST-type radar in the troposphere over Santa Cruz, Costa Rica

Marcial Garbanzo-Salas[1,2*] and Wayne Hocking[2]

Abstract

Results from the first VHF profiler research radar in Costa Rica, operating at a central radar frequency of 46.6 MHz, are presented. Emphasis has been on studies of scattering layers detected in the altitude range 1–6 km, with the main goal being to identify regions with radar echoes and observe the temporal evolution of the echoes. Data were obtained over the course of a full year using a vertical resolution of better than 100 m. Layers of strong scatter were observed regularly, often with simultaneous broad spectra, which may indicate enhanced turbulence. Similar layers have been observed over equatorial Indonesia, and these have been associated with the planetary boundary layer. The presence of echo layers was more common during the dry-season months (December–April); in fact during March, two layers were observed in the lower troposphere for more than 35% of the time. Stable pattern structures often occurred for extended periods, but at times the layers could also vary drastically in behavior from 1 day to the next. After sunset, strong echo layers could persist for several hours. Some examples of regularly observed layer behavior are given.

Keywords: MST type radar, Planetary boundary layer, Layers of turbulence

Introduction

During the past few years an initiative to create a radar research center has been undertaken in Costa Rica. The location chosen for the radar site is a satellite campus of the University of Costa Rica located in Santa Cruz (Lat: 10.283720, Lon: −85.595166, Elevation: 60 m a.s.l). Santa Cruz provides the project with a quiet radio-frequency environment and sufficient land to expand the arrays or deploy other instruments if the need arises. In Costa Rica there were no tropospheric radars before this project started. Consequently, this was the first time that a VHF radar could be used to obtain detailed information about tropospheric behavior and structure.

The radar operates at a central frequency of 46.6 MHz and was designed for low-altitude (1–6 km) studies. It comprises a group of 9 Yagi-antennas for transmission, and clusters of 4 antennas for reception. Initially only one receiver cluster was used, but this was subsequently upgraded into a three-receiver system. Several aspects of Costa Rica's radar design and location enhance its research capabilities (Hocking et al. 2014). In North America, bandwidth allocations to radar operators are usually limited to typically 250 kHz for radars operating at central frequencies of ∼ 20–60 MHz. However, for the Costa Rica radar, a bandwidth allocation of 5 MHz was assigned to the project. An immediate advantage of the large bandwidth is that the spectral content of the pulse sent into the atmosphere can contain a wide range of frequencies. In the case of the radar in Santa Cruz, this bandwidth was used by creating a several MegaHertz wide chirp frequency inside the pulse.

Pulses were coded using a chirped frequency which varied linearly from the start to the end of the pulse by 2 MHz. Deconvolution was used to greatly improve the range resolution (Hocking et al. 2014). In order to carry out the deconvolution, the signal of the transmitted pulse was recorded along with the received signal. A radar pulse with a length of 1 km (3.336 μ s) should have

*Correspondence: marcial.garbanzo@ucr.ac.cr
[1] CIGEFI, University of Costa Rica, 2060 San Pedro, San José, Costa Rica
Full list of author information is available at the end of the article

a resolution of 500 m, but by introducing the deconvolution, the resolution was improved to less than 100 m. This improvement in resolution, coupled with the relatively long pulse, resulted in strong, well-defined echoes from the atmosphere, even with a low power transmitter. The radar used a 1 kW peak-power transmitter to gather information satisfactorily up to 6 km. The pulse repetition frequency was 3 kHz, and a 64-point coherent integration scheme was also used. The total data-length per dataset was 20 s.

Another feature of this radar was that the hardware used in the detection was minimized. Only one detector per channel of digitization was used; normally two are required for in-phase and quadrature signals, but our use of high sampling rates (comparable to the radio frequency) and deconvolution procedures means that the in-phase and quadrature components could be generated in software after digitization on a single channel (Hocking et al. 2014). Each detector consisted of just 4 amplification stages and one filtering circuit. No mixing or beating took place in hardware, minimizing addition of extra electronic noise and artificial frequency content.

Several different experiments took place during the years 2013–2014 and more than 190 complete days covering almost a full year were recorded and later analyzed. Here we present results of analysis of powers, spectral widths and other related parameters.

Results are presented in two main categories, these being (1) category I events, which refer to quasi-striated (layered) atmospheric echoes, and (2) category II events, which refer to echoes likely to be associated with the planetary boundary layer (PBL from now on). Typical examples as well as more detailed statistics are presented for each category.

Methodology

In this section, different methodologies are described. Our spectral analysis is described first, followed by discussion of the processes of obtaining information about the atmospheric echoes, their evolution, and their classification.

We will refer to "atmospheric targets", which will be taken to be any radar-scattering entity generated by natural atmospheric events which result in radio-backscatter detectable by the radar. Aircraft and man-made targets are not considered, and clearly signals that are too weak to be detected will not be included either. Lightning is also excluded in our case. We also exclude meteors (which can appear in our data due to range-aliasing) and transient phenomena.

To begin, we look at Doppler spectral analysis. Initially the received signal is deconvolved with the signal of the transmitted pulse (Hocking et al. 2014). Doppler spectra are then estimated from the time series using a fast Fourier transform (FFT). Doppler peaks can be related to properties of atmospheric targets.

Details about spectral peak location and determination can be found in many references, e.g., Yamamoto et al. (1988), Hocking (1997), so we will not discuss these procedures in detail here. We have used a Gaussian fitting method, in which we fit a function of the form $f(v) = A\, e^{\frac{-(v-v_o)^2}{2\sigma^2}} + D$ to the spectra. The variables A, v_o, σ and D were determined using a nonlinear least squares fitting method. A is the peak value of the fitted Gaussian function, and v_o is the offset of the peak from zero Doppler shift (in units of meters per second). The value of σ is associated with the width of the associated spectral peak and is related in part to the velocity distribution of turbulence and hence the turbulent energy dissipation rate, e.g., Jacoby-Koaly et al. (2002), although consideration of the impact of so-called spectral beam-broadening is also very important, e.g., Hocking (1983). The value of D represents the noise level. The total integrated power under the atmospheric contribution to the spectrum was also determined in our analysis (after removal of noise) and was used as the main measure of backscattered power in this paper.

After the spectral analysis was finished, the information was compiled and studied in order to observe the atmospheric behavior for each day, since the radar echoes and their temporal evolution can teach us about different atmospheric processes. The sequence used for the analysis of each daily dataset consisted of several basic steps:

1. Observe general aspects of the day (long lasting echoes, strong echoes, isolated patches of intense returns, and their time evolution).
2. Identify echo layers based on integrated power, spectral width, and radial velocity.
3. Measure layer durations.
4. Match the layers observed with other phenomena observed on the current (and even previous) day(s).
5. Identify possible PBL behavior based on integrated power, spectral width, and radial velocity.
6. Characterize the boundary layer by its maximum depth and growth rate.
7. Identify regions of strong isolated backscattering (also referred to as "isolated patches of turbulence", or IPoTs).
8. Measure the horizontal extent of the IPoTs to quantify their presence in the atmosphere.
9. Note any interesting events, transitions, or patterns.

This methodology was carried out for each of the available daily datasets. In this manner the information was

quantized and statistics were calculated about the presence of echo layers, characteristics of the PBL and isolated patches of turbulence (IPoTs). The IPoTs (characterized by a lack of structure as they were not layers or organized events) will not be treated in this paper, as more research is needed in order to better understand their morphology, time evolution and to provide possible interpretations.

Moving our focus on to regions of persistent returns, the methodology used to quantify scattering layer occurrence will now be discussed. Of course it is possible that layers did occur which were too weak to be seen by the radar, either due to weak turbulence, or due to the layers being very well mixed, leading to weak backscatter. The latter were referred to as "ghost layers" by Hocking et al. (2016), who also discussed the reasons for their existence, and such layers have been modeled by Fritts et al. (2012). However, we do note that data recorded by Luce et al. (2002) do indicate that such layers are likely to be rare—usually most turbulent layers produce some degree of backscatter. In order to be specific, we will tend to use the name "echo layers" to discuss radio-detected scattering layers, to help emphasize the types of layers we are detecting.

In regard to our classification scheme, we have based it on the number of echo layers measured and the fractional portion of the day during which they were present. We will discuss category I echoes (layered, or striated echoes) first, then layers associated with the PBL (category II). Within each category, various classes will be defined.

Category I: layered echoes

We first discuss category I echoes. These scattering layers generally formed and died at roughly the same height, showing little sustained ascent or descent. They are also at times referred to as "striated" echoes. These were subdivided into 3 sub-categories (referred to as "classes"), based on the number of occasions when one, two, and three or more quasi-horizontal echo layers were observed simultaneously. These classes were denoted L1, L2, and L3, respectively. This type of analysis was carried out for all the available days in the radar dataset. The length of time for which each layer was observed was also recorded.

However, radar scatter may not always be isotropic, and could even be anisotropic (possibly due to wind-shear effects and production of quasi-specular reflectors), thus leading to narrower spectra. For this reason we also carefully determined the spectral widths associated with the echoes, and used wide spectral widths as a proxy for enhanced turbulence. In general, spectral widths were quite wide for category I echo layers, so that in the main the association of these echoes with turbulence seems justifiable.

Category II: PBL

Turning our attention to the top of the PBL, it can be expected that this region should be a region of enhanced turbulence and consequently should be detectable by radar. The PBL grows in depth throughout the day, so the associated echoes should ascend from low heights in mid-morning to greater heights as the day unfolds. We did indeed observe echo layers at heights consistent with the likely tops of the PBL, in line with this assumption. These often rose in altitude quickly with time and could persist for several hours, in line with expected PBL behavior. We also note here that we use the term PBL in a general sense: a PBL can be either convective or stably stratified, but either has some potential to produce radar backscatter as long as suitable refractive index variations exist. So while we expect that many of the layers are convective PBL (often denoted CBL); we will not make that distinction here.

In such cases where the behavior and movement of the layers were consistent with this expected behavior, we used the echo layers as a proxy for PBL behavior. Such behavior is consistent with the observations of Hashiguchi et al. (1995), for example.

The echoes associated with the PBL do not appear so much as a "layer" in height-time contour plots, but rather as rising echoes, but of course in physical space they would have extended over many tens or hundreds of km, and so would in fact be a physical layer. At times, additional category I echoes could be seen to evolve from the residual motions of the PBL, and these were counted as layers in our category-I analyses.

Just as with category I echoes, studies of the spectral widths were important in helping determine whether the scatter was from turbulence. Category II echoes generally appeared to be turbulent.

Two classes of echoes associated with the PBL were created. The first class included those cases in which the layering and temporal behavior could be considered as relatively "typical". The second class incorporated echoes which exhibited behavior that was uncommon. The uncommon cases are not shown here but can be found elsewhere (Garbanzo-Salas 2015).

These different echoes are discussed in the next section.

Results and discussion

Layered echoes

Figure 1 shows examples of integrated power, spectral width and radial velocity for a single day (April 13th, 2014), highlighting category I-type echoes. Below about

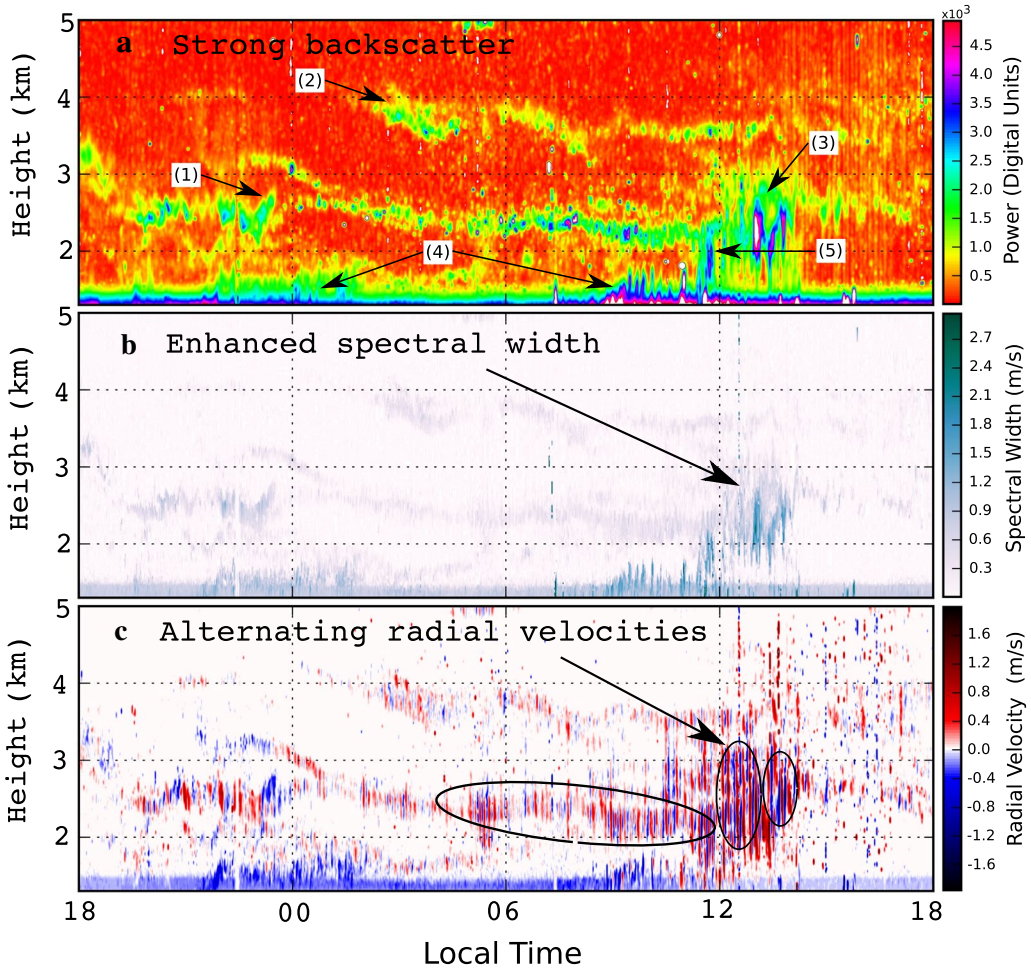

Fig. 1 Radar product used for analysis. Information obtained by Gaussian fitting to the Doppler spectra. Shown are **a** integrated power, **b** spectral width, and **c** radial velocity for April 13th, 2014. This type of product was generated for each day and used to categorize and classify the atmospheric echoes by recognizing various different characteristics and their associated time evolution

1.2 km altitude some receiver saturation is observed, but it has been included because it helps show the lower limits of the useable data.

Two strong and persistent category I echo layers, labeled (1) and (2) in the figure, can be seen around mean altitudes of approximately 2.5 and 3.5 km, respectively, though varying in height throughout the day by ± several 100 m. Echo layer (1) is prominent throughout the full 24-h period; layer (2) starts well before sunrise and persists for a significant portion of the remaining day. Both layers are associated with enhanced spectral width [see panel (b)], suggesting significant sub-pulse-scale vortical and/or fluctuating motions (convection and/or turbulence). Spectral widths can reach as high as 1 m s^{-1} in these cases. Just prior to noon, and persisting till just after 2 pm, the whole region from 1 to 3.5 km altitude produced strong backscatter [labeled (3)], with layer (1) broadening substantially in depth and almost merging with a layer below. Also of interest is the fact that the vertical velocities [panel (c)] alternated between positive and negative values at several times [particularly in layer (1)], indicating either wave activity or some sort of organized vertical convection with large up-welling and down-welling. The oscillations have a mean period of 7.65 min between 05:00 and noon (encircled by the long flat ellipse), of 11.47 min just prior to noon (first vertical ellipse), and changing to about 12.08 mins toward the end of the oscillatory period (second vertical ellipse). These latter two values are close to the expected Brunt–Väisälä period. We will not dwell specifically on these oscillations, but they are certainly of interest and worthy of more detailed future study. They might be of value in determining mean temperature gradients, e.g., see (Röttger 1980).

Below the altitude of 2.0 km, enhanced echoes are observed between ∼ 22:00 and 02:00 LT and between

∼ 08:00 and 12:00 [labeled (4)], but since no data are evident below 1 km altitude, it is unclear if these are layers, or the top of a convective region extending up from the ground. The vertical extrusions in region (4) are suggestive of vertical plumes.

The enhanced scatter just before 12:00 [labeled (5)] seems distinct from regions (1) and (4). It apparently merges with the turbulent layer (1) at around 2.5 km. There is a possibility that it may be the signature of turbulence associated with the growth of a convective boundary layer or a shallow PBL.

We now turn to a longer dataset consisting of nine consecutive days. This is shown in Fig. 2. Multiple striated echo layers were observed regularly during this period. Data from April 6th to the 8th clearly show multiple striated quasi-horizontal layers, with more than three layers visible simultaneously at different heights. For example, the layers on April 7th persisted for ≈ 60% of

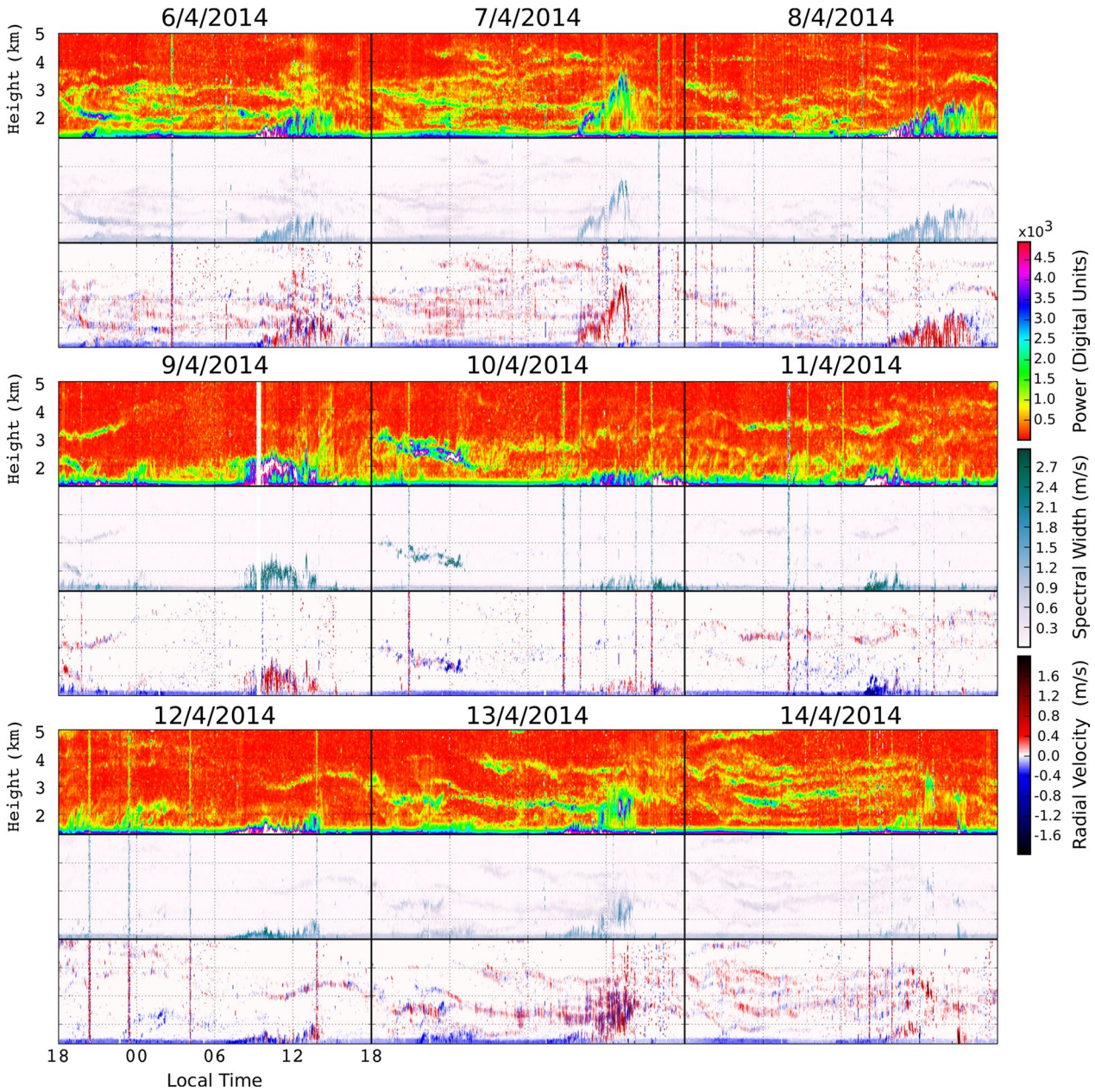

Fig. 2 Radar products for nine consecutive days, from April 6th to April 14th (2014). Three days per panel are shown with the dates specified at the top. Each day contains three graphs, these being (from top to bottom) (1) Integrated power, (2) Spectral width, and (3) Radial Velocity. The amount of time when no echo layer is observed is scarce. On occasions as many as five simultaneous echo layers could be observed (e.g., April 14th)

the day (14.2 h), and they were allocated to class **L3** in our scheme. A case with one layer can be observed at the 12 h mark of April 12th. This case was classed as an **L1** case with a duration of 0.46 of a day (11.04 h).

Note in the data for April 7th, a region of strong echoes can be seen rising from 1 km altitude just prior to noon and reaching heights of almost 4 km by mid-afternoon. This is *not* a category I echo, but rather a category II echo, and will be discussed shortly. Other examples appear on April 8th and 13th.

The data displayed in Fig. 2 are representative of the dry season (typically December to April).

Results of the statistics gathered about echo layers will now be presented. However it is worth first clarifying that June 2014 was missing in the analysis due to data storage issues. Furthermore, July, August and November (2014) registered less than 10 days of useful data per month. However, information is presented as a fraction of the total measured time, so the values given below for these months are still considered to be representative, albeit with larger uncertainties than the other months.

Statistics obtained with the L1/L2/L3 classification scheme are now presented in Fig. 3. Here, (and also Fig. 5—to come later), all relevant statistics were obtained using all three parameters of power, spectral width and vertical velocity. The primary parameter used was the power, but spectral width and vertical velocity were used as backup information in determining things like echo lifetime and confirming that the character of the layer had not changed during its duration.

It is clear that the presence of striated echo layers is greater during the dry season. The minimum percentage of time during which only one layer was found during the dry-season months occurred in May, with 15.6% occurrence. A maximum of 32.1% temporal coverage of all type L1 layers was observed during February. The L2 class had largest occurrence during March with 37.2%, while the L3 class maximized in the following month of April, reaching a monthly maximum of 24.2%. Figure 3 shows that there seems to be a local minimum in echo layers observed in July, although it must be remembered that there were no data in June.

PBL echoes

We now turn our attention to category II echoes. As noted above, examples could be seen on April 7th, 8th and 13th, but better examples are shown in Fig. 4. Figure 4a shows a very clear example, which has been emphasized by adding a broken line to guide the eye. It is also labeled as "(1)". The echoes rise out from the lowest heights and ascend throughout the day. All graphs in Fig. 4 show similar events, except for Fig. 4c.

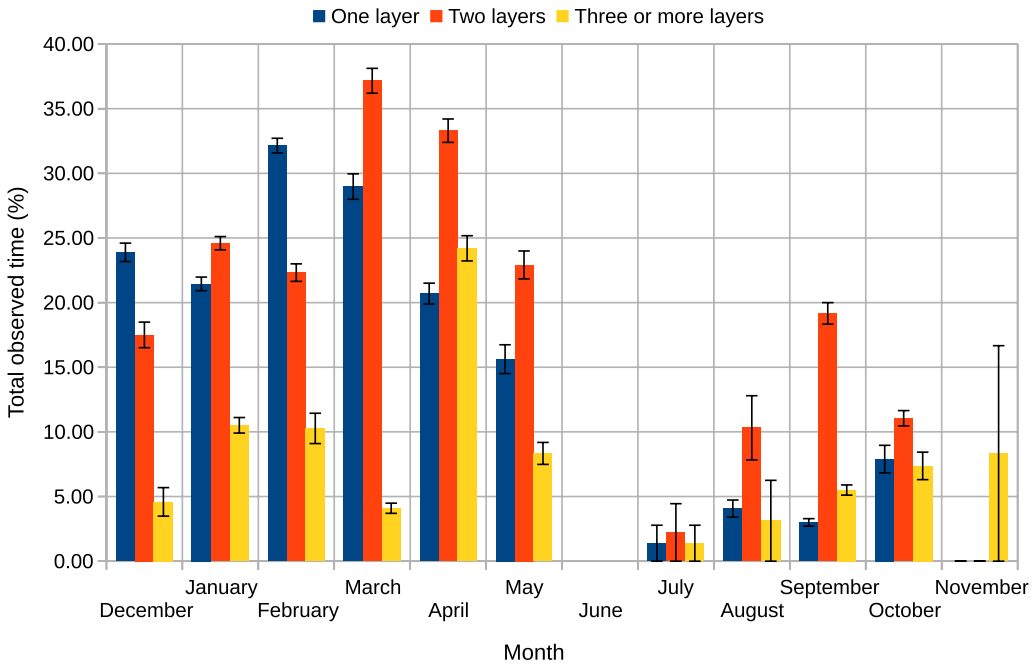

Fig. 3 Echo layer results. Year-long statistics of atmospheric layers. One (L1), two (L2), or more than two (L3) echo layers were observed, and the percentage of time that each type of layering persisted within each month (relative to available radar time) is presented. The maximum value is reached during the dry-season months. The rainy season shows a decrease in the number of measurable layers. Error bars represent ± 1 standard deviation

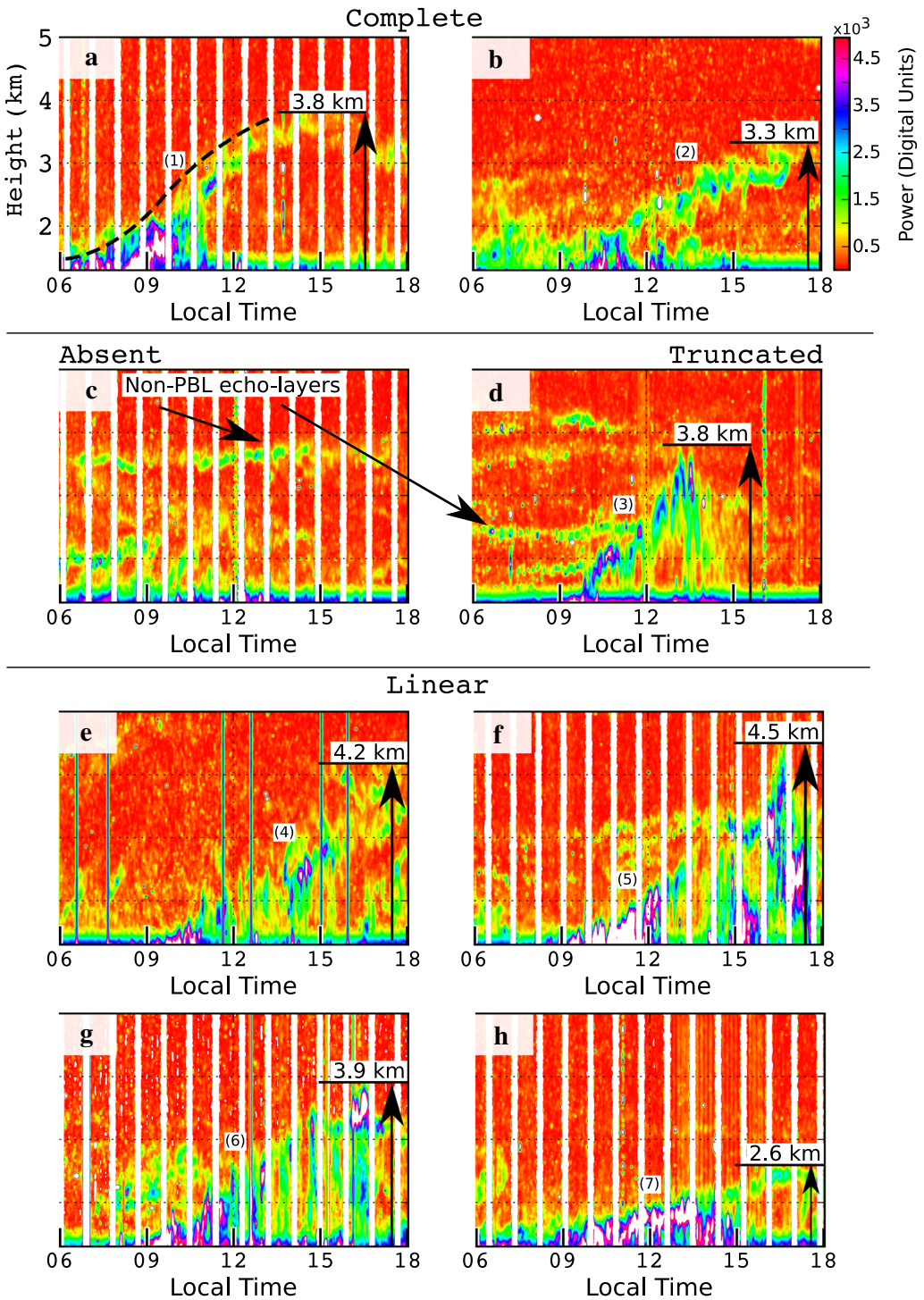

Fig. 4 Typical common echo layer structures. Eight different cases of likely PBL evolution are shown, labeled (1) to (7). Panels **a** and **b** [cases (1) and (2)] correspond to continuous growth with full development of the PBL echoes as observed on February 18th, 2014 and December 28th, 2013, respectively. Panel **c** shows the case of February 8th, 2014 where no observable PBL echoes were found. Panel d) contains a case of truncated linearly growing PBL echoes (3) observed on April 7th, 2014. Cases for January 9th, May 4th, March 11th and February 13th (2014 for all the cases) are presented in panels **e**, **f**, **g**, and **h**, as (4), (5), (6), and (7), respectively, and exemplify linear growth of the echoes at the top of the PBL top. Note that the layers generally have different ascension rates

Cases of category I echoes in Fig. 4 are indicated as "non-PBL echo layers"; these have been discussed above and will not be considered further here.

Although all PBL echoes show similar general behavior, appearing in the mid-morning at around 1 km altitude and rising steadily, they do vary in detail. Figure 4 shows examples of different types of evolution, labeled from (1) to (7). Strong quasi-linear growth can be observed during April 7th, while more modest growth rates can be observed during other days (e.g., April 6th, 8th and 9th). Examples of the PBL maximum heights are also marked in Fig. 4. For example, in Fig. 4e, the maximum is marked as 4.2 km, this being the upper level of the echoes associated with the PBL. However, one could argue that this might be too high, and some of these echoes, while strong, might actually lie above the PBL top. However, we also examined spectral widths for these echoes, and they were quite wide, indicating turbulence. They could of course be small plumes rising out of the PBL, but at present we cannot distinguish that. Hence we will persist with our determinations of height in this way, using the upper levels of enhanced turbulence associated with these PBL echoes, in order to at least maintain a consistent definition. We see annual variability of over 1.5 km, which is greater than any uncertainty associated with measurements on any 1 day, thus making these data still of value.

Over 80% of days showed PBL-type layers. The classes contained in Fig. 4 (primarily category II echoes) are described in more detail here:

- *Continuous growth with full development* Figure 4a contains data for February 18th, 2014. At the maximum rate of growth the PBL top rises in altitude by ~ 12 cm s^{-1} and reaches a maximum height of 3.8 km. Figure 4b displays the case recorded during December 28th, 2013. A clear PBL top is observed to grow, but with weaker backscatter strength than the previous case. After reaching a maximum of 2.9 km the height remains approximately constant until it decays away near sunset (18:00 h).
- *Absent* On some occasions there are no echo layers growing from the lower heights. Figure 4c contains a representative case of this situation, showing data for February 8th, 2014.
- *Truncated* Figure 4d, taken from data corresponding to April 7th, 2014, shows a clear echo layer with linear growth that rose steadily in height at a rate of 14 cm s^{-1} for several hours and then suddenly disappeared at 3.75 km altitude at a time of 01:35 pm.
- *Linear growth* Figure 4e–h shows different cases of linear growth corresponding to January 9th, May 4th, March 11th and February 13th (in all cases for the year of 2014). The four cases are presented to cover the most common scenarios observed for this type of growth. The echo layers for the first three cases (e–g) correspond to linear growth with vertical ascent speeds of 9.1, 10.1 and 9.6 cm s^{-1}. A large difference between the three cases is evident underneath the layers. Figure 4e) presents a region of weak scattering (red coloring) under the layer top, in the body of the PBL. The cases presented in Fig. 4f and g do not show such a "radar-quiet" region below the layer top. Instead strong echoes are observed in the f panel before sunset and less intense echoes are observed in the g panel, both with similar behavior. These differences will be discussed shortly. The last case presented in Fig. 4h contains a linear but rather weak growth of the layer top. An ascension rate of 3.3 cm s^{-1} was estimated for this case, which represents close to one third of the estimated value for the other three cases just described. In this case, even with a slow growth, a region of only weak scattering below the layer top is observed, similarly to Fig. 4e.

As discussed above, while the top of the PBL seems to be associated with enhanced echoes, the region below the top, and down toward the ground (referred to here as the "body" of the PBL) often generates little to no backscatter, especially when the growth is continuous. Panels a and b in Fig. 4 are examples, but this feature occurs at times for all types of category II echoes. Yet on other occasions strong scatter from the body of the PBL can be seen. When scatter is weak from the body of the PBL, it may suggest weak turbulence, but it is also possible that the air in this region has been homogenized by the turbulence, resulting in weak backscatter despite enhanced turbulence (e.g., see earlier discussions about "ghost layers"). This is an area for future study, but it is important to remark that the PBL echo layer growth rates are not particularly dependent on the absence or otherwise of scatter from the body of the PBL.

In the previous paragraphs, several representative cases of echo layers were described. Of course not all the cases observed during the year-long experiment were as clearly defined or as simple to describe as the ones just discussed, but for the well-defined cases we had sufficient data to allow determination of useful statistics.

Minimum, maximum and average heights of the ascending echo layer top were calculated for each month and are graphed in Fig. 5. The monthly means represent averages of daily means, and standard deviations of the daily values were also found and plotted on the graph as vertical "error bars", these representing ± 1 half standard deviation. As seen, the average height was at a minimum

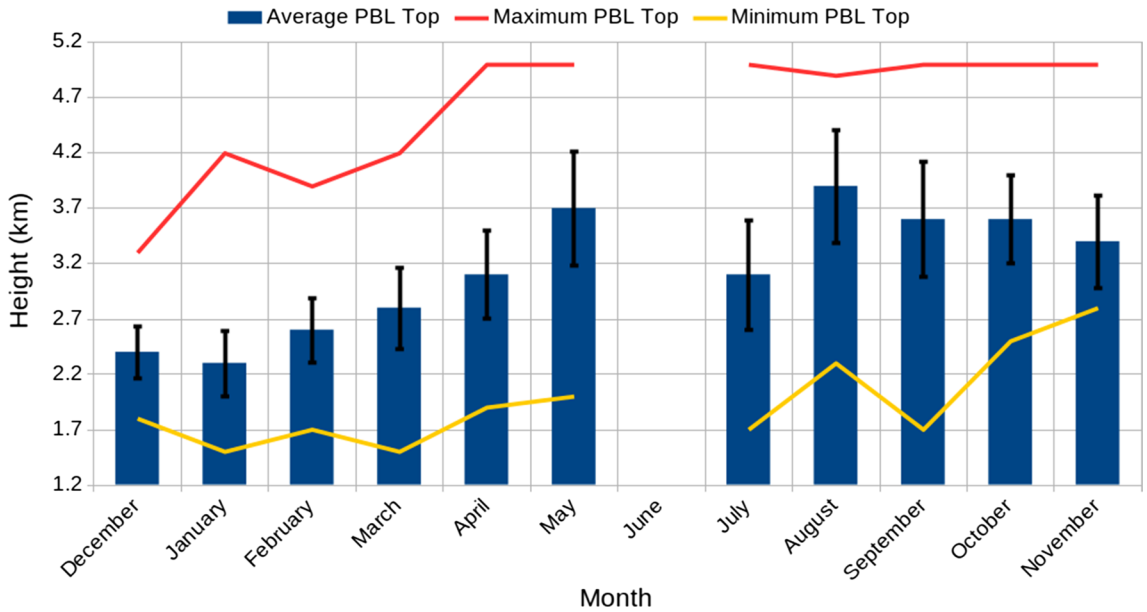

Fig. 5 PBL echo layer results. The heights of the tops of the PBL as a function of month, using our echo layers as a proxy for PBL. The average value of the PBL per month, as well as the maximum and minimum heights observed for individual days, is shown. The average PBL top is at the greatest heights during May and August. A local minimum is observed during July, while the yearly minimum value was registered during January. The variability is shown as black vertical line bars which represent ± half standard deviation

during the dry season and maximized during the rainy season. The maximum height of the layer top often reached the 5 km maximum measurable height during the rainy season months. These cases were often associated with discrete layers or convection (not shown).

The month of July (as observed in Fig. 5) shows a decrease in the average height of the ascending layer top. This decrease could be due to the limited data available for this month, but there is also the possibility that the July dataset is impacted by a phenomenon known in Central America as veranillo. Also known as Midsummer Drought (Magaña et al. 1999), it is a multi-component event in which atmospheric conditions imitate the dry-season months (December-April). This similarity to dry-season atmospheric behavior could cause the average height to tend more to dry-season altitudes in July.

Figure 5 shows that the average height reached a yearly maximum of 3.93 km during August. The minimum was registered during January, which showed a mean monthly height of 2.34 km. The $\approx$ 1.6 km difference between rainy and dry season average is large and represents a net increase of 68% penetration higher into the troposphere. This increase in depth can be caused by more (and/or stronger) ascending air currents and less wind shear generated by weakened easterly winds from the Caribbean sea. The minimum (yellow line) observed in Fig. 5 seems less conclusive regarding the observed maximum during the rainy season.

Other scatterers

Our focus in the last sub-section has been (to a large extent) on cases where the layers actually appear to be markers for the PBL and convective boundary layers (and especially their tops). However, we have already discussed other types of scatterers (e.g., iPOTs) and of course the striated echoes, which may be largely independent of the PBL. However, the various layers can also be mixed. For example, we have discussed the occurrence of cases where category I layers have "spun off" the PBL. In other cases, even PBL-type layers can show odd behavior. For example, on April 12th (see the data on the bottom panel of Fig. 2), a weak category II layer could be interpreted as occurring at midnight. Later on the same day, at noon, a striated layer located at 3 km is displaced upwards to 3.5 km and falls back to 3 km after 2.5 h. These types of activity seem to have nothing to do with the PBL, which was lower down so certainly other dynamics are at play there.

We have concentrated on events which can be fairly clearly defined to satisfy one of our two categories: these other events represent areas of research for future study.

Conclusions

The VHF profiler radar located in Santa Cruz, Costa Rica, has been used to probe the lower troposphere. The three parameters of backscattered power, spectral width and radial velocity have been combined

to identify and characterize the atmospheric echoes. Strong backscatter was observed regularly in the form of layers. These layers generally were stable in height with time (to within ± 1 km or so) and were referred to as category I echoes.

However, on many days echoes were observed ascending in time after mid-morning, and decaying near sunset. These echoes seem to be well associated with the PBL, and in particular seem to highlight the top of the PBL. We have referred to them as category II echoes, and have taken them to be proxies for PBL height. Further verification should nonetheless be undertaken using other instruments like radiosondes, and such radar/in situ comparisons will be the subject of future research.

Figures 1, 2, and 4 show representative layers, while results of statistical analyses are given in Figs. 3 and 5. Figure 3 considers category I echoes (layers) and shows frequencies of occurrence of days in which (i) 1, (ii) 2 and (iii) 3 or more layers (referred to as L1, L2, and L3 classes, respectively) existed simultaneously. The most frequent occurrence of such layers was observed to be in the middle of the dry season, during February [for the one layer (L1) case] and March [for the two layer (L2) case]. The least frequent occurrence of layers in our data occurred during July (for all the categories, though recognizing that we had no data for June).

Figure 5 shows the mean heights of the PBL layers and their variability. We are especially interested in their heights because they are a measure of the depth of the PBL. The minimum average height occurs during January and the maximum during August, suggesting that minimum depths of the PBL generally occur during the dry season and the maxima occur during the rainy season. A local minimum in July could be correlated with the regional veranillo phenomenon.

More measurements are needed to establish a robust climatology and to appropriately confirm this relationship between layers and seasonal rain distribution.

The experimental data reported in this paper were obtained with the radar in "stand-alone" mode, and there were no backup instruments, so some of the findings need further investigation. A new experiment is underway to obtain similar data for 2017–2018. During 2019 a 2-month campaign of radiosonde launches will be carried out at the radar site. This campaign will allow us to improve the radar operation and gather more information for the analysis and interpretation of radar echoes.

Authors' contributions

The theory and code were developed jointly, and both authors contributed to the data gathering, processing, analysis and writing of this paper. All authors have contributed to the interpretation of the results.Both authors read and approved the final manuscript.

Author details

[1] CIGEFI, University of Costa Rica, 2060 San Pedro, San José, Costa Rica. [2] University of Western Ontario, 1151 Richmond Street, London, Canada.

Acknowlegements

Thanks to the University of Costa Rica for the funds assigned to the Projects B1107 and B1108, the University of Western Ontario for the time and support for the field trips, and Mardoc for providing some equipment and antennas. This work was made possible by the facilities of the Shared Hierarchical Academic Research Computing Network (SHARCNET: www.sharcnet.ca) and Compute/Calcul Canada.

Availability of data and materials

Due to the large size of the dataset it would be provided on demand to the corresponding author.

Competing interests

The authors declare that they have no competing interests.

Funding

The funds for this research were provided by the University of Western Ontario, The Natural Sciences and Engineering Council of Canada, and the University of Costa Rica.

Publisher's Note

Received: 28 February 2018 Accepted: 4 January 2019
Published online: 15 January 2019

References

Fritts DC, Wan K, Franke PM, Lund T (2012) Computation of clear-air radar backscatter from numerical simulations of turbulence: 3. Off-zenith measurements and biases throughout the lifecycle of a Kelvin–Helmholtz instability. J Geophys Res Atmos 117(D17):17101

Garbanzo-Salas M (2015) High resolution tropospheric studies with an MST type radar. Ph.D. thesis, The University of Western Ontario

Hashiguchi H, Fukao S, Tsuda T, Yamanaka MD, Tobing DL, Sribimawati T, Harijono SWB, Wiryosumarto H (1995) Observations of the planetary boundary layer over equatorial Indonesia with an L band clear-air Doppler radar: initial results. Radio Sci 30(4):1043–1054

Hocking WK (1983) On the extraction of atmospheric turbulence parameters from radar backscatter Doppler spectra: I. Theory. J Atmos Terr Phys 45:89–102

Hocking WK (1997) System design, signal-processing procedures, and preliminary results for the Canadian (London, Ontario) VHF atmospheric radar. Radio Sci 32(2):687–706

Hocking WK, Hocking A, Hocking DG, Garbanzo-Salas M (2014) Windprofiler optimization using digital deconvolution procedures. J Atmos Sol Terr Phys 118:45–54

Hocking WK, Röttger J, Palmer RD, Sato T, Chilson PB (2016) Atmospheric radar: application and science of MST radars in the earth's mesosphere, stratosphere, troposphere, and weakly Ionized regions. Cambridge University Press, Cambridge, pp 662–663

Jacoby-Koaly S, Campistron B, Bernard S, Bénech B, Ardhuin-Girard F, Dessens J, Dupont E, Carissimo B (2002) Turbulent dissipation rate in the boundary layer via UHF wind profiler Doppler spectral width measurements. Bound Layer Meteorol 103(3):361–389

Luce H, Fukao S, Dalaudier F, Crochet M (2002) Strong mixing events observed near the tropopause with the MU radar and high-resolution balloon techniques. J Atmos Sci 59(20):2885–2895

Magaña V, Amador Ja, Medina S (1999) The midsummer drought over Mexico and Central America. J Clim 12(6):1577–1588

Röttger J (1980) Structure and dynamics of the stratosphere and mesosphere revealed by VHF radar investigations. Pure Appl Geophys 118:494–527

Yamamoto MK, Sato T, May PT, Tsuda T, Fukao S, Kato S (1988) Estimation error of spectral parameters of mesosphere–stratosphere–troposphere radars obtained by least squares fitting method and its lower bound. Radio Sci 23:1013–1021